A Simple Algorithm to Discriminate between Meteorological and Nonmeteorological Radar Echoes

JOHN M. KRAUSE

Cooperative Institute for Mesoscale Meteorological Studies, University of Oklahoma, and NOAA/OAR/National Severe Storms Laboratory, Norman, Oklahoma

(Manuscript received 28 October 2015, in final form 15 June 2016)

ABSTRACT

Discriminating between meteorological and nonmeteorological radar returns is necessary for a number of radar applications, including hydrometeor classification, quantitative precipitation estimation (QPE), and the computation of specific differential phase K_{DP}. The algorithm proposed, MetSignal, uses polarimetric radar data and is simple by design, allowing users to adjust its performance based on the location's specific needs. The MetSignal algorithm is a fuzzy logic technique with a few postprocessing rules and has been selected for implementation on the WSR-88D network in the United States.

1. Introduction

Data from single- and dual-polarization weather radars are used in a wide variety of applications. The first step in these applications is the separation of data that contain meteorological signals from that which contain nonmeteorological signals (Gourley et al. 2007). The performance of applications such as quantitative precipitation estimation (QPE; e.g., Tang et al. 2014), the computation of specific differential phase K_{DP} (e.g., Wang and Chandrasekar 2009), and many others are dependent on accurate identification of the locations of meteorological signals. The problem is complicated by the fact that the variety and types of nonmeteorological echoes [such as those from insects, birds, clutter, and anomalous propagation (AP)] rival those of meteorological echoes (such as those from hail, graupel, snow, and rain); many types of nonmeteorological scatterers exhibit similar radar characteristics to those of meteorological scatterers (e.g., Straka et al. 2000; Kumjian 2013a,b,c). The algorithm described in this paper—MetSignal—is scheduled for incorporation into the WSR-88D system on the Open Radar Product Generator (ORPG) as part of build 17, which is scheduled for deployment in late 2016. The output from the MetSignal algorithm will be used in the ORPG to identify meteorological signal locations for the computation of K_{DP} and QPE.

The development and deployment of dual-polarization radar allows meteorologists to better discriminate between meteorological and nonmeteorological scatterers using information about the scatterers' shape and phase via differential reflectivity Z_{DR} and the diversity of particle types via cross-correlation coefficient ρ_{hv} (Park et al. 2009). The current approach in the ORPG is to use ρ_{hv} greater than 0.9 as the threshold to identify regions of meteorological signal (Ryzhkov et al. 2005). This approach can fail to identify meteorological signal in hail cores and areas within the melting layer, where ρ_{hv} may be less than 0.9 (e.g., Straka et al. 2000; Zrnić et al. 1993; Giangrande and Ryzhkov 2008; Ryzhkov et al. 2013). Using the above-mentioned threshold ($\rho_{hv} > 0.9$) can also lead to false detections of meteorological signal for areas of AP and biological scatterers (Tang et al. 2014). Because radar reflectivity factor at horizontal polarization Z_h is also high in AP, QPE creates significant amounts of false precipitation from this error (Berenguer et al. 2006).

The current scientific literature contains numerous approaches from a variety of authors that deal with the problem of identifying and removing nonmeteorological signal or classifying each return as a particular hydrometeor type (e.g., Zrnić and Ryzhkov 1999; Zrnić et al. 2001; Berenguer et al. 2006; Park et al. 2009; Tang et al. 2014; Bechini and Chandrasekar 2015; Wen et al. 2015). The proposed algorithm differs from these methods in two important ways. First, many of the algorithms in the

Corresponding author address: John Krause, RRDD, NSSL, 120 David L. Boren Blvd., Norman, OK 73072-7319.
E-mail: john.krause@noaa.gov

DOI: 10.1175/JTECH-D-15-0239.1

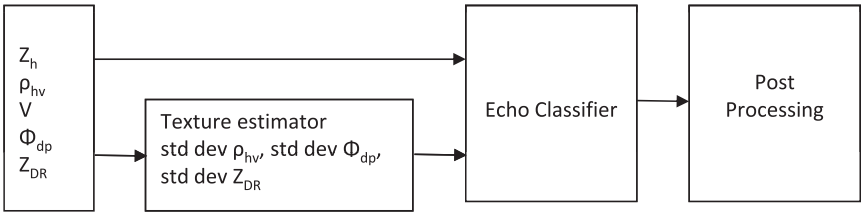

FIG. 1. Block diagram of meteorological signal algorithm.

current literature attempt to deal with the difficulty of the problem by becoming increasingly complex, using sophisticated neural networks (e.g., Lakshmanan et al. 2014) or complex and lengthy multistep processes (e.g., Bechini and Chandrasekar 2015) that are both computationally intensive to operate and difficult to implement or optimize (e.g., Wen et al. 2015). Second, complex algorithms incorporate data from other observing systems and/or data from the radar volume in its entirety to carefully refine their calculations. In contrast, the proposed algorithm—MetSignal—is simple to implement, easy to optimize, and offers improved computational speed and simplicity. It relies only on dual-polarization radar data. Because the proposed method is planned for deployment on the operational WSR-88D network, errors found in the method postdeployment are difficult to correct. If a neural network or other complex algorithm is deployed on the WSR-88D, retraining or modifying the algorithm to correct for postdeployment errors can change the results in unexpected ways. With the proposed method, a predictable correction of errors can be attempted by adding additional postprocessing rules.

2. Method

A comprehensive summary of echo classification methods can be found in Chandrasekar et al. (2013). Following this work, Fig. 1 summarizes the major steps of the proposed algorithm as a block diagram. The selection of variables and the weights given to those variables are identified in Table 1 and will be discussed in a following section. The inputs to the echo classifier are Z_h, ρ_{hv}, radial velocity V, standard deviation of differential phase [std dev(Φ_{DP})], standard deviation of differential reflectivity [std dev(Z_{DR})], and standard deviation of cross-correlation coefficient [std dev(ρ_{hv})]. The standard deviations of the variables are computed from the data collected along a radial for nine range bins centered on the bin of interest. Note that they could also be computed using a 2D box centered on the range bin of interest or with many other techniques.

The method applied for echo classification is a weighted fuzzy logic scheme. This is a common technique, applied by many others for hydrometeor classification (e.g., Park et al. 2009). The weighted fuzzy logic scheme used here is a simple form with only a single output class—meteorological signal. The weights W assigned to each input are provided in Table 1. Most of the membership functions (Fig. 2) are single-sided trapezoids, but the V membership function is a two-sided inverted trapezoid, the value of which can be computed by subtracting its inverse trapezoid from 1.

The aggregation value A is determined at each bin as follows:

$$A = \frac{\sum_{j=1}^{6} W_j \mathrm{PV}_j}{\sum_{j=1}^{6} W_j},$$

where W_j is the weight and PV_j is the value of the membership function of the jth input. The aggregation value is then compared to a threshold between 0 and 1 to determine whether the signal is meteorological. The threshold used in this study is 0.8 in the warm season and 0.7 in the cold season, and its selection is discussed in a following section.

After the aggregation value has been computed, a few postprocessing rules are applied. First, locations where the absolute value of Z_{DR} exceeds 4.5 dB are considered nonmeteorological. This rule was developed to assist the algorithm in properly classifying migrating birds and wind turbine clutter. Second, locations where ρ_{hv} is less than 0.65 are also considered nonmeteorological. Finally, the algorithm checks the value of Z_h at a height of

TABLE 1. The six variables and the weight assigned to each in the MetSignal algorithm.

Variable	Weight
Horizontal reflectivity Z_h	1.0
Cross-correlation coefficient ρ_{hv}	1.0
Velocity V	1.0
Variability of differential phase [std dev(Φ_{DP})]	2.0
Variability of differential reflectivity [std dev(Z_{DR})]	2.0
Variability of cross-correlation coefficient [std dev(ρ_{hv})]	1.0

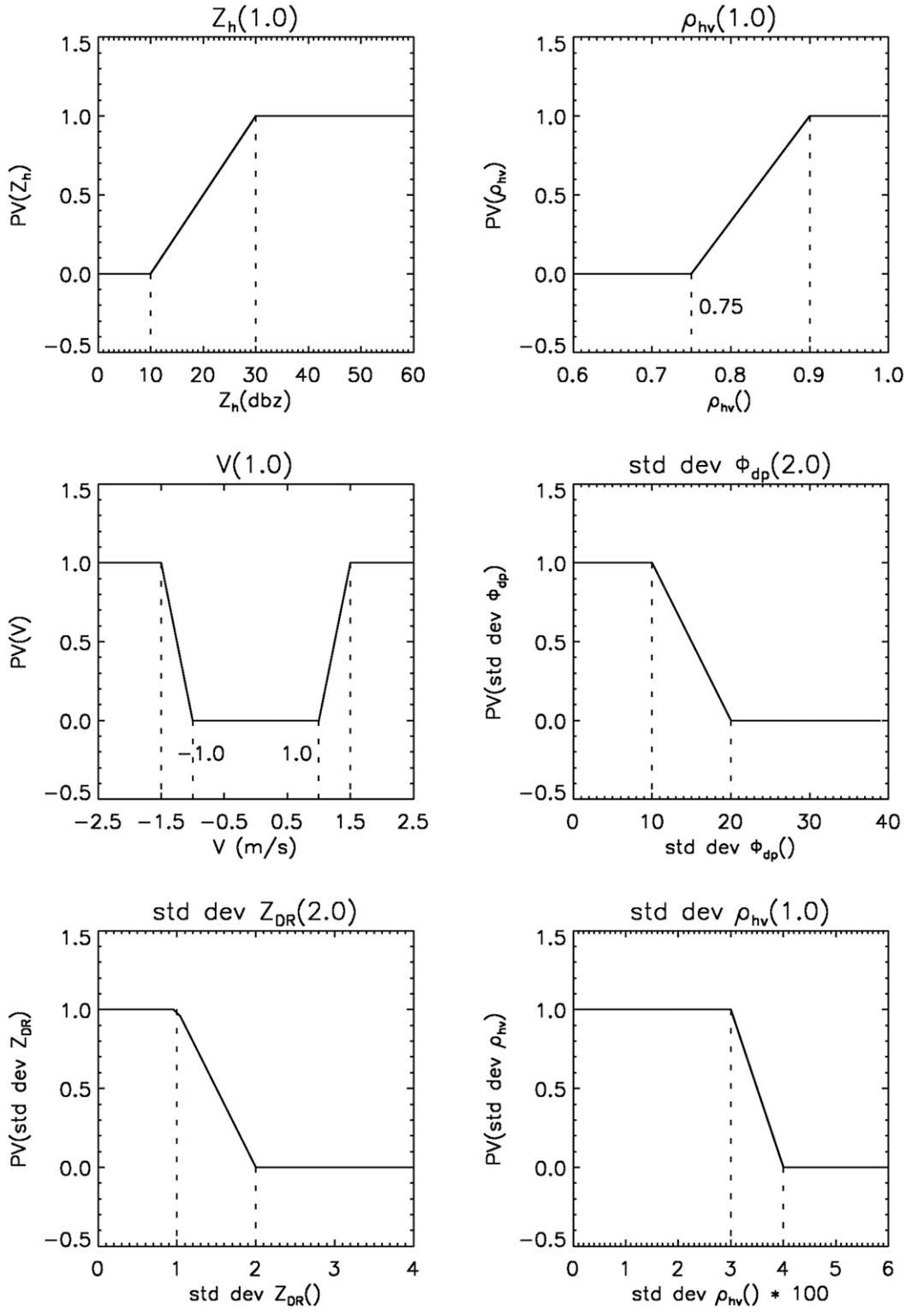

FIG. 2. The six membership functions of the MetSignal algorithm: Z_h, ρ_{hv}, V, std dev(Φ_{DP}), std dev(Z_{DR}), and std dev(ρ_{hv}). The numbers in parentheses at the top of the graphs are the W used for that variable. PV(·) is the value of the membership function for a given input.

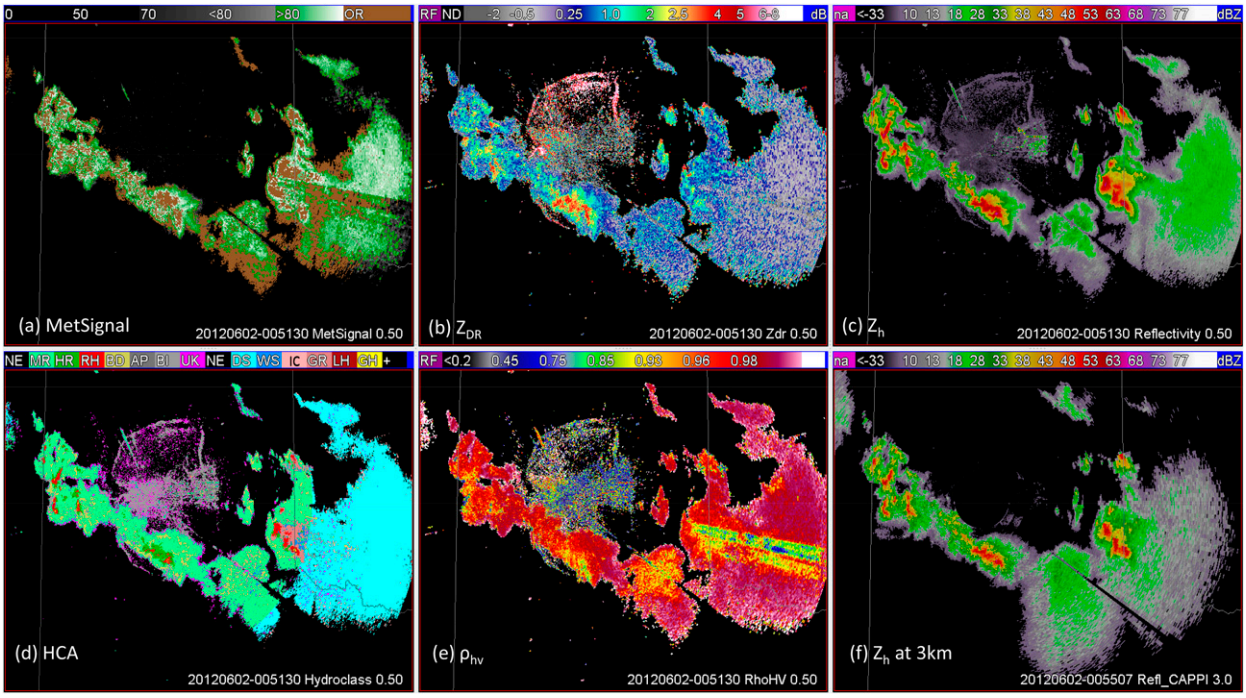

FIG. 3. (a) MetSignal, (b) Z_{DR} (dB), (c) Z_h (dBZ), (d) HCA, (e) ρ_{hv}, and (f) Z_h (dBZ) at 3 km. All from the KAMA WSR-88D radar at 0051 UTC 2 Jun 2012 from an elevation of 0.5°. HCA output classes are labeled as light rain (LR), heavy rain (HR), rain/hail mixture (RH), big drops (BD), anomalous propagation (AP), biological (BI), unknown (UK), no echo (NE), dry snow (DS), wet snow (WS), ice crystals (IC), graupel (GR), large hail (LH), and giant hail (GH).

3 km in the previous volume scan at the sample location. If this value exceeds 11 dBZ, then the location is considered to be meteorological (Lakshmanan et al. 2015). This addition assists the algorithm in correctly identifying precipitation in the melting layer, where many of the computed texture functions are elevated.

3. Results

Radars located on the Great Plains in the central United States can sample a wide variety of meteorological and nonmeteorological targets within a single elevation. In Fig. 3, the KAMA radar located near Amarillo, Texas, observed multiple large-hail-producing storms, as well as fine lines from storm outflows, anomalous propagation, ground clutter, wind turbine clutter, second-trip echo, and a large (but common) area near the radar filled with insects. An examination of the ρ_{hv} field (Fig. 3e) reveals that the thunderstorms to the east-southeast of the radar (at ~100° azimuth) have a significant amount of nonuniform beamfilling (Ryzhkov 2007) that can be identified by the radial streaks of lower ρ_{hv}. There is also a strong melting layer signature in the data found to the south-southeast of the radar (at ~150° azimuth). These locations are marked as ''OR'' for override (brown) by the MetSignal algorithm. This means that the data were originally marked as nonmeteorological, but this designation was overridden and changed to meteorological because the Z_h at 3-km field (Fig. 3f) exceeded the threshold of 11 dBZ in postprocessing. At the time specified in the figure, many of the meteorological data come from rapidly developing thunderstorms, which contain higher values of the texture variables std dev(Φ_{DP}), std dev(Z_{DR}), and std dev(ρ_{hv}). High texture values lead to lower scores in the membership functions and consequently lower aggregation values. The logic of the MetSignal algorithm seeks to identify meteorological signal only where there is strong evidence and relies on postprocessing to add back in those locations where a missed detection is likely to have occurred. The power of this approach can be seen in the locations near the radar, where very few insects have been misclassified as meteorological echoes, and to the east of the radar, where AP and fine lines from outflow boundaries have been properly classified as nonmeteorological echoes. The hydrometeor classification algorithm (HCA; Park et al. 2009) often misclassifies insects and AP in locations near the radar with a variety of false alarms, such as big drops (BD), light rain (LR), or even hail (SH). This can be seen in Fig. 3d. Finally, it should be noted that the MetSignal algorithm does not remove the elongated second-trip echo located to the northwest of the radar. This is due to the fact that

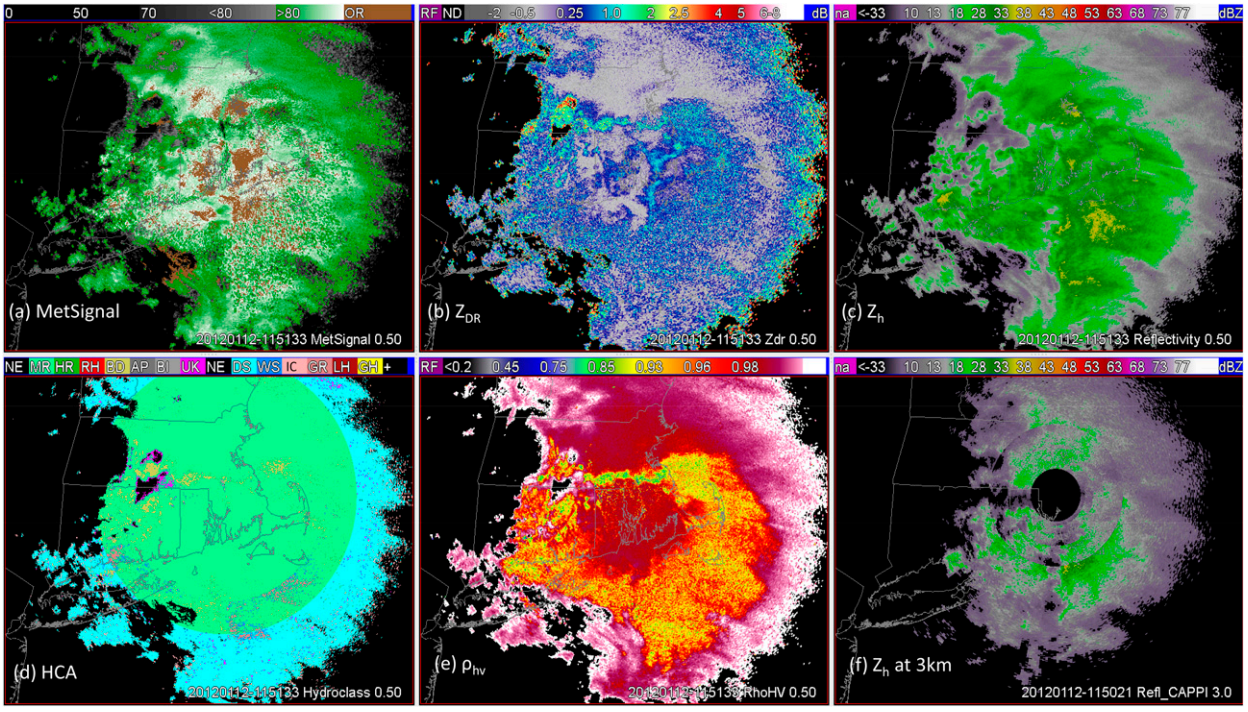

FIG. 4. (a) MetSignal, (b) Z_{DR} (dB), (c) Z_h (dBZ), (d) HCA, (e) ρ_{hv}, and (f) Z_h (dBZ) at 3 km. All from the KBOX WSR-88D radar at 1151 UTC 12 Jan 2012 from an elevation of 0.5°. HCA output classes as in Fig. 3.

second-trip data have characteristics identical to meteorological returns.

In winter events, there are typically fewer nonmeteorological targets like insects, but strong melting layer signals, which are noisy, can confuse fuzzy logic algorithms (Bechini and Chandrasekar 2015). Figure 4 shows a winter storm, sampled by the KBOX radar, near Boston, Massachusetts, on 12 January 2012; a strong melting layer signature can be seen in Fig. 4e. The melting layer is especially strong just to the north of the radar as an elongated east-to-west band. MetSignal (Fig. 4a) and the HCA (Fig. 4d) properly classify a majority of signal present as meteorological and have difficulty only in areas where there is a strong melting layer. An examination of the OR class in Fig. 4a again demonstrates the design of the MetSignal algorithm to flag locations as meteorological only when a strong meteorological signal is present and then to use the $Z_h \geq 11$ dBZ at 3 km criterion to reduce missed detections.

Limitations of the method can be found in Fig. 5, which is a collection of nonmeteorological targets from different locations in the United States. The first pair of images is MetSignal (Fig. 5a) and HCA (Fig. 5b) from KJAX in Jacksonville, Florida, for a period with very strong bird returns. There is no precipitation in the area at this time. The HCA is contaminated with detections of BD and a few LR misclassifications on the edges of the echo. MetSignal shows a few misclassifications to the northwest of the radar, but a larger issue is the ringlike OR classifications mainly to the southwest. These are due to the Z_h at 3 km being in excess of 11 dBZ, which causes the nonmeteorological fuzzy logic classification to be overridden in postprocessing. The ringlike appearance is due to the data coming from a different (lower) elevation as it is interpolated to 3 km (note that similar elevation rings in Z_h at 3 km can be found in Fig. 4f). One possible way to optimize the MetSignal algorithm for KJAX might be to increase the height at which the OR classification operates (e.g., from 3 to 4 km). This same limitation of the MetSignal algorithm is shown in the pair of images (Figs. 5c,d) from KHDX in Holloman, New Mexico. MetSignal suppresses most of the spurious AP and biological returns, but the smoke from a fire triggers the OR classification for the area just to the northeast of the radar. Ground returns from atmospheric ducting are also likely to be incorrectly identified as meteorological by the algorithm to the south. The pair of images (Figs. 5e,f) from KICT in southern (Wichita) Kansas shows strong AP to the north and west with true meteorological return in the south. Wind turbine clutter is also common at this location. MetSignal does a good job suppressing nonmeteorological detections while also identifying the storms to the south as meteorological. Some AP is flagged by the algorithm as

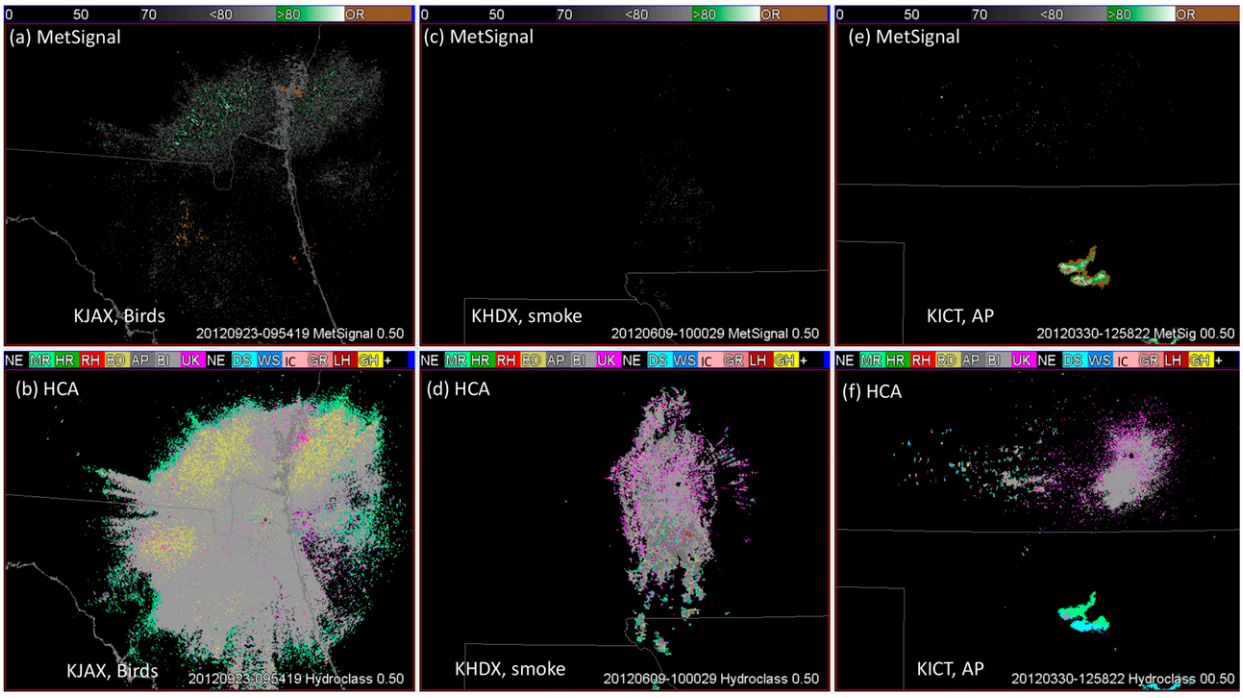

FIG. 5. A comparison of the performance of MetSignal and HCA for various nonmeteorological targets. (a) MetSignal and (b) HCA for KJAX at 0954 UTC 23 Sep 2012 with contamination by birds. (c) MetSignal and (d) HCA for KHDX at 0733 UTC 9 Jun 2012 with mountain clutter and smoke. (e) MetSignal and (f) HCA for KICT at 1247 UTC 30 Mar 2012 with strong AP and wind turbine clutter. HCA output classes as in Fig. 3. All data are collected from an elevation of 0.5°.

meteorological signal again due to strong Z_h returns at a height that would be 3 km in the standard atmosphere.

The computational efficiency of the MetSignal algorithm was compared to the algorithm proposed by Tang et al. (2014). In a test on data from the KAMA radar located near Amarillo, Texas, from 0000 to 0100 UTC 2 June 2012, the MetSignal algorithm was ~10 times faster than the dual-polarization radar reflectivity quality control (dpQC) algorithm proposed by Tang et al. (2014); on the author's computer, the MetSignal algorithm spent ~2400 ms in the computational sections of the algorithm versus ~26 000 ms for dpQC as proposed by Tang et al. (2014).

4. Discussion

The selection of variables and the weights given to those variables is critical to the success of MetSignal. An example of the process used in the design of the MetSignal algorithm can be found in Figs. 6 and 7. In Fig. 6, an area of nonmeteorological signal is highlighted with a blue polygon, and an area of meteorological signal is highlighted with a green polygon. Data were then extracted from each area and analyzed. The data included the six dual-polarimetric radar moments—horizontal reflectivity, differential reflectivity, velocity, spectrum width (SPW), differential phase, and cross-correlation coefficient—and a measure of the variability (standard deviation) of each moment using a centered nine-gate sample of the data along the radial. In all, 12 different data fields were considered. The characteristics of the data were evaluated using histograms. The six data fields selected for inclusion in the algorithm (Fig. 7) show consistent separation between meteorological and nonmeteorological histograms for the 25-plus cases in the dataset (Table 2). Following the work of Lakshmanan et al. (2015) and experience in the application of the Park et al. (2009) algorithm, Z_{DR} was excluded because of possible radar miscalibration in the WSR-88D network.

The design of the membership functions and the selection of variable weights followed an iterative process. Initial estimates for both the shape of the membership functions and the weights for the variables were assumed. The MetSignal algorithm was computed and run on the cases in our dataset (Table 2). The algorithm was then assessed, and areas of poor performance were identified. Data were extracted from those areas and evaluated, the results of which drove changes to the membership functions and the variable weights. Figure 7 shows the final membership functions that resulted from our iterative process (red

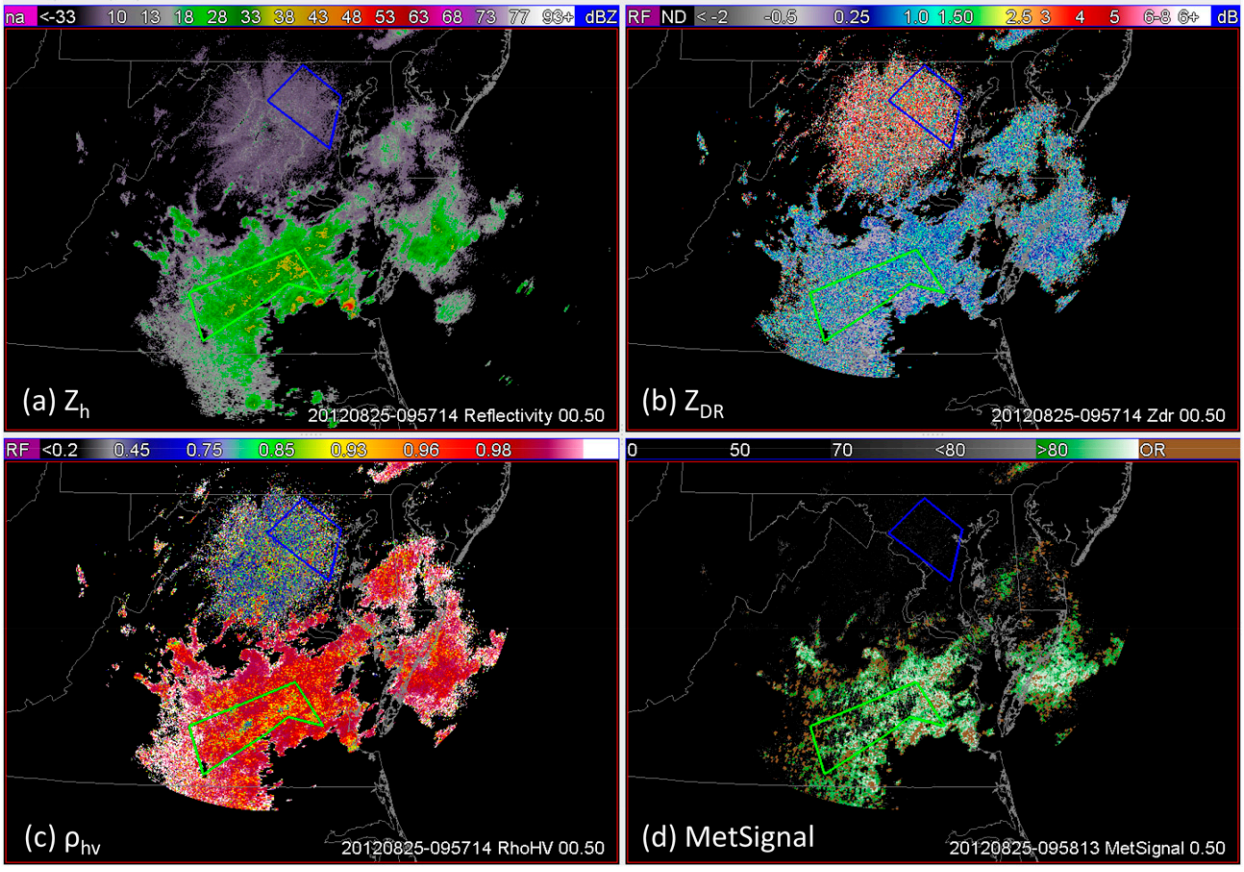

FIG. 6. A display of (a) Z_h (dBZ), (b) Z_{DR} (dB), (c) ρ_{hv}, and (d) MetSignal from KLWX at 0911 UTC 25 Aug 2012 from an elevation of 0.5°. The green polygon designates an area of meteorological signal, and the blue polygon designates an area of nonmeteorological signal.

lines) and the matching normalized histograms from the data (blue and green lines) identified in Fig. 6. Biological scatterers, mainly insects, which are very common in the WSR-88D network during the warm season, are the major nonmeteorological contaminant in the data.

Five of the six final variables in Fig. 7 show good separation between the histograms for nonmeteorological (blue) and meteorological (green) data for this case. The histograms for velocity do not show good separation; there is a significant amount of overlap for both nonmeteorological and meteorological data. This is because moving insects are the dominant nonmeteorological scatterer in this case. Velocity is not particularly useful for separating the data for this case. However, for other cases in the dataset, such as those that have ground clutter and AP, velocity adds meaningful discriminating power.

The weight of each variable (Table 1) indicates our expectation of that variable's importance. A primary finding of Lakshmanan et al. (2015) was that the variance (texture herein) of Z_{DR} had the most value in discriminating between meteorological and nonmeteorological signals. We can confirm this and our iterative process described above assigned std dev(Z_{DR}) a weight of 2.0. Although std dev(Φ_{DP}) was not studied by Lakshmanan et al. (2015), the performance of this measure is likely similar to that of K_{DP}—lower in meteorological data and higher in nonmeteorological data. The std dev(Φ_{DP}) showed a strong separation between meteorological and nonmeteorological histograms for all of our cases and was also assigned a weight of 2.0. Many algorithms such as the current ORPG and Tang et al. (2014) use ρ_{hv} as the primary or only measure of meteorological signal. We have included it as both ρ_{hv} and the texture of ρ_{hv}. Each has a weight of 1.0 but combined they are equal in importance to both the texture of Z_{DR} and the texture of Φ_{DP}. Usually, ρ_{hv} and std dev(ρ_{hv}) are statistically linked wherein if ρ_{hv} approaches 1.0, then the std dev(ρ_{hv}) is usually low (meteorological) and as ρ_{hv} drops below 0.75, then std dev (ρ_{hv}) usually rises (nonmeteorological) (Melnikov and

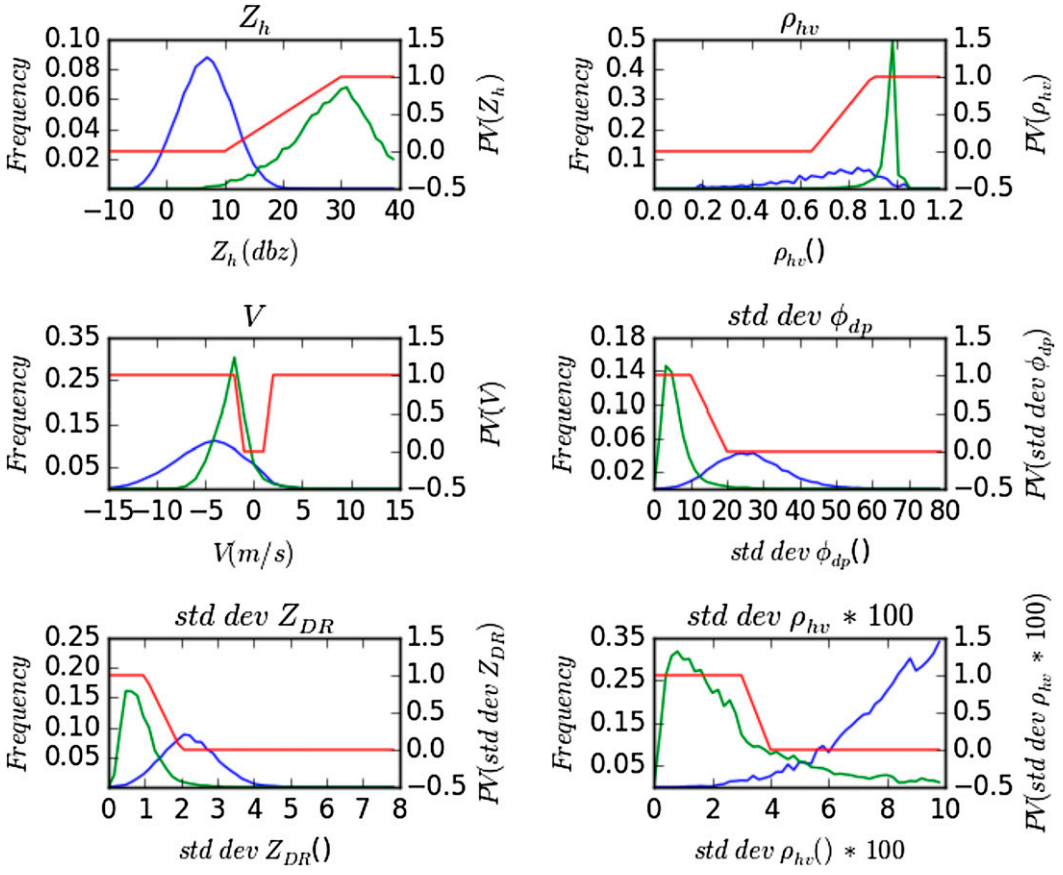

FIG. 7. Normalized histograms of data from different regions identified in Fig. 6 are overlaid onto the six membership functions (red lines) of the MetSignal algorithm. Normalized histograms from the nonmeteorological region are shown in blue. Normalized histograms from the meteorological region are shown in green.

Zrnić 2007). Finally, two variables are included that have smaller weights; V, with a weight of 1.0, was included to identify areas of the domain where the beam may be hitting the ground (which usually results in V of $\sim 0\,\mathrm{m\,s^{-1}}$); and Z_h was included with a weight of 1.0 to help identify locations with hail and locations within the melting layer. In general, the approach was to use the texture values (low) and ρ_hv to identify meteorological locations.

All of the cases in Table 2 were studied before a threshold of A that was best able to separate meteorological and nonmeteorological signals could be identified. It was evident from the data that a more stringent threshold should be applied in summer, when more nonmeteorological signal was present from birds and insects, than in winter, when there was relatively less nonmeteorological return. The threshold of 0.80 was used for periods of the year when biological targets (e.g., insects) are most commonly present, and 0.70 was used during the cold season, when biological contamination is less likely. Figure 8 shows the normalized histograms for the MetSignal algorithm output for the data regions identified in Fig. 6. The threshold of 0.80 appears to be quite strict for this case. In other cases, the stricter threshold of 0.80 is necessary to reduce false detections owing to contamination from birds in the MetSignal output. Figure 9 is a set of normalized histograms from three locations where bird contamination is present. The threshold of 0.80 is effective in classifying almost all of the signal from birds as nonmeteorological.

The change in threshold from 0.80 in summer to 0.70 in winter works in tandem with the postprocessing application of $Z_\mathrm{h} \geq 11\,\mathrm{dB}Z$ at 3 km [a threshold suggested by Lakshmanan et al. (2015)]. The value of Z_h used in this postprocessing step is kept from the previous volume scan by storing the data from each elevation that is closest to the constant altitude of 3 km [i.e., a constant-altitude plan position indicator (CAPPI) is created]. The threshold of $Z_\mathrm{h} \geq 11\,\mathrm{dB}Z$ at 3 km is used to infer a vertical depth to the radar echo, which is strong evidence of a meteorological signal. In summer, storm heights are expected to be greater than in winter owing to typically greater convective potential

TABLE 2. Data used to develop and test the MetSignal algorithm.

Radar	Location	Date	Description
KAKQ	Wakefield, VA	22 Jun 2012	Weather mixed with insects
KAMA	Amarillo, TX	1 Jun 2012	Severe storms with nonweather targets
KATX	Seattle, WA	7 Mar 2012	Weather and mountains
KBGM	Binghamton, NY	11 Aug 2012	Light snow
KBMX	Birmingham, AL	16 Jan 2013	Winter precipitation
KBOX	Boston, MA	1 Dec 2012	Winter storm
KCLE	Cleveland, OH	14 Dec 2011	Winter precipitation
KCLE	Cleveland, OH	11 Aug 2012	Ground clutter only
KDIX	Philadelphia, PA	22 Apr 2012	Sea clutter/weather
KDOX	Dover Air Force Base, DE	22 Apr 2012	Weather/birds/strong clutter
KHDX	Holloman, NM	6 Sep 2012	Ground clutter/mountains/smoke
KICT	Wichita, KS	30 Mar 2012	Wind turbine/ground clutter
KJAX	Jacksonville, FL	23 Sep 2012	Birds
KLOT	Chicago, IL	29 Jun 2012	Ground clutter/storms
KLWX	Sterling, VA	17 Jul 2012	Insects
KLWX	Sterling, VA	21 Aug 2012	Insects/storms
KLWX	Sterling, VA	25 Aug 2012	Insects/storms
KLWX	Sterling, VA	11 Oct 2012	Birds
KLWX	Sterling, VA	1 Nov 2012	Insects/storms
KMLB	Melbourne, FL	26 Jan 2012	Biological/storms
KMPX	Minneapolis, MN	10 Oct 2012	Strong birds
KMPX	Minneapolis, MN	8 Nov 2012	Biological/storms
KNQA	Memphis, TN	21 Sep 2012	Ground clutter/mesoscale convective system
KPBZ	Pittsburg, PA	26 Jan 2012	Winter storm
KPBZ	Pittsburg, PA	28 Nov 2011	Winter storm
KPBZ	Pittsburg, PA	8 Nov 2012	Ground clutter
KVNX	Vance Air Force Base, OK	8 Dec 2011	Bats

instability, so the application of a strict threshold (0.80) can be corrected if detections are missed. In the cold seasons, when biological contamination is relatively low, storm-top heights are also generally lower and postprocessing will be unable to assist the fuzzy logic classification, so a lower threshold of 0.70 is recommended.

Many combinations of fuzzy logic thresholds and postprocessing techniques can be used, depending on

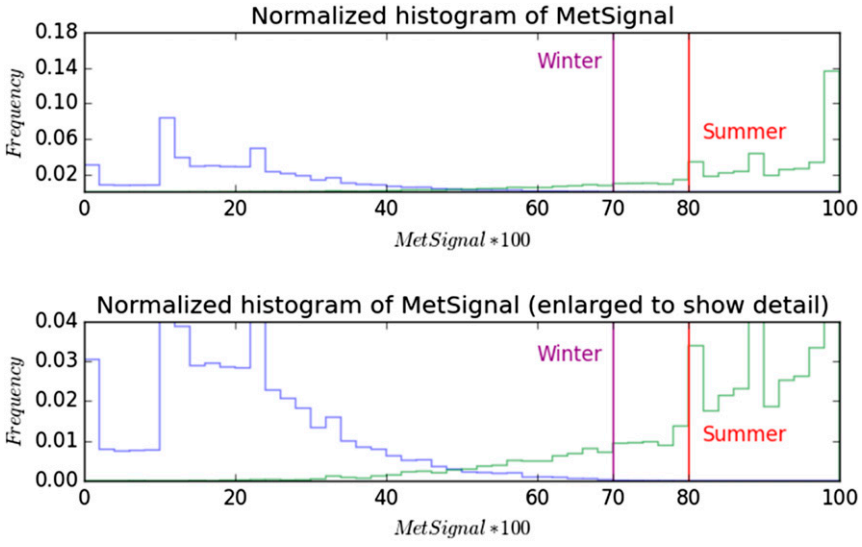

FIG. 8. Normalized histograms of MetSignal from the different regions identified in Fig. 6. The normalized histogram from the nonmeteorological region is blue, while the meteorological region is green. The red line shows the threshold value of 80 [= 0.8(100)] used in summer, and the purple line shows the threshold value of 70 [= 0.7(100)] recommended for winter. Both panels contain the same data, but the bottom had the *y* axis adjusted to show detail.

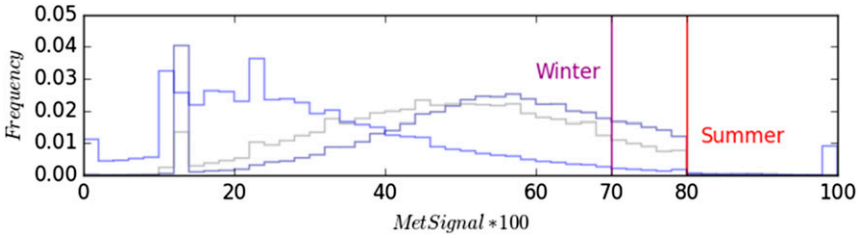

FIG. 9. Normalized histograms of MetSignal from three different locations where bird contamination was present. The blue line is from KJAX (Jacksonville, FL) on 23 Sep 2012. The gray line is from KLWX (Sterling, VA) on 11 Oct 2012. The dark blue line is from KMPX (Minneapolis, MN) on 10 Oct 2012. The red line shows the threshold value of 80 [= 0.8(100)] used in summer, and the purple line shows the threshold value of 70 [= 0.7(100)] recommended for winter.

the location and types of nonmeteorological contaminants expected. If the algorithm is applied in regions where light and/or winter precipitation is normal, then the lower aggregation threshold is recommended. If the algorithm is applied in regions where terrain blocks the radar beam, then the addition of a terrain map may prove useful. As described, the MetSignal algorithm provides good discrimination between meteorological and nonmeteorological returns for a wide variety of conditions.

5. Conclusions

A simple fuzzy logic algorithm was developed to separate meteorological and nonmeteorological radar echoes. This algorithm uses only dual-polarization weather radar data and a few simple postprocessing rules, and is scheduled for implementation on the WSR-88D ORPG in late 2016. It relies on fuzzy logic, simplicity of optimization, and enhanced computational speed over more technically complex solutions that use a wider variety of data and logic.

Acknowledgments. The author would like to thank Dr. Jeff Snyder for his encouragement and assistance in the preparation of this manuscript, and Dr. Alexander Ryzhkov for his helpful suggestions during algorithm development. Funding was provided by NOAA/Office of Oceanic and Atmospheric Research under NOAA–University of Oklahoma Cooperative Agreement NA11OAR4320072, U.S. Department of Commerce.

REFERENCES

Bechini, R., and V. Chandrasekar, 2015: A semisupervised robust hydrometeor classification method for dual-polarization radar applications. *J. Atmos. Oceanic Technol.*, **32**, 22–47, doi:10.1175/JTECH-D-14-00097.1.

Berenguer, M., D. Sempere-Torres, C. Corral, and R. Sánchez-Diezma, 2006: A fuzzy logic technique for identifying nonprecipitating echoes in radar scans. *J. Atmos. Oceanic Technol.*, **23**, 1157–1180, doi:10.1175/JTECH1914.1.

Chandrasekar, V., R. Keränen, S. Lim, and D. Moisseev, 2013: Recent advances in classification of observations from dual polarization weather radars. *Atmos. Res.*, **119**, 97–111, doi:10.1016/j.atmosres.2011.08.014.

Giangrande, S. E., and A. V. Ryzhkov, 2008: Estimation of rainfall based on the results of polarimetric echo classification. *J. Appl. Meteor. Climatol.*, **47**, 2445–2462, doi:10.1175/2008JAMC1753.1.

Gourley, J. J., P. Tabary, and J. P. du Chatelet, 2007: A fuzzy logic algorithm for the separation of precipitating from nonprecipitating echoes using polarimetric radar observations. *J. Atmos. Oceanic Technol.*, **24**, 1439–1451, doi:10.1175/JTECH2035.1.

Kumjian, M. R., 2013a: Principles and applications of dual-polarization weather radar. Part I: Description of the polarimetric radar variables. *J. Oper. Meteor.*, **1**, 226–242, doi:10.15191/nwajom.2013.0119.

——, 2013b: Principles and applications of dual-polarization weather radar. Part II: Warm- and cold-season applications. *J. Oper. Meteor.*, **1**, 243–264, doi:10.15191/nwajom.2013.0120.

——, 2013c: Principles and applications of dual-polarization weather radar. Part III: Description of the polarimetric radar variables. *J. Oper. Meteor.*, **1**, 226–242, doi:10.15191/nwajom.2013.0119.

Lakshmanan, V., C. Karstens, J. Krause, and L. Tang, 2014: Quality control of weather radar data using polarimetric variables. *J. Atmos. Oceanic Technol.*, **31**, 1234–1249, doi:10.1175/JTECH-D-13-00073.1.

——, ——, ——, K. Elmore, A. Ryzhkov, and S. Berkseth, 2015: Which polarimetric variables are important for weather/no-weather discrimination? *J. Atmos. Oceanic Technol.*, **32**, 1209–1223, doi:10.1175/JTECH-D-13-00205.1.

Melnikov, V. M., and D. S. Zrnić, 2007: Autocorrelation and cross-correlation estimators of polarimetric variables. *J. Atmos. Oceanic Technol.*, **24**, 1337–1350, doi:10.1175/JTECH2054.1.

Park, H., A. Ryzhkov, D. Zrnić, and K.-E. Kim, 2009: The hydrometeor classification algorithm for the polarimetric WSR-88D: Description and application to an MCS. *Wea. Forecasting*, **24**, 730–748, doi:10.1175/2008WAF2222205.1.

Ryzhkov, A. V., 2007: The impact of beam broadening on the quality of radar polarimetric data. *J. Atmos. Oceanic Technol.*, **24**, 729–744, doi:10.1175/JTECH2003.1.

——, S. Giangrande, and T. Schuur, 2005: Rainfall estimation with a polarimetric prototype of WSR-88D. *J. Appl. Meteor.*, **44**, 502–515, doi:10.1175/JAM2213.1.

——, M. Kumjian, S. Ganson, and P. Zhang, 2013: Polarimetric radar characteristics of melting hail. Part II: Practical implications. *J. Appl. Meteor. Climatol.*, **52**, 2871–2886, doi:10.1175/JAMC-D-13-074.1.

Straka, J. M., D. S. Zrnić, and A. V. Ryzhkov, 2000: Bulk hydrometeor classification and quantification using polarimetric radar data: Synthesis of relations. *J. Appl. Meteor.*, **39**, 1341–1372, doi:10.1175/1520-0450(2000)039<1341:BHCAQU>2.0.CO;2.

Tang, L., J. Zhang, C. Langston, J. Krause, K. Howard, and V. Lakshmanan, 2014: A physically based precipitation–nonprecipitation radar echo classifier using polarimetric and environmental data in a real-time national system. *Wea. Forecasting*, **29**, 1106–1119, doi:10.1175/WAF-D-13-00072.1.

Wang, Y., and V. Chandrasekar, 2009: Algorithm for estimation of the specific differential phase. *J. Atmos. Oceanic Technol.*, **26**, 2565–2578, doi:10.1175/2009JTECHA1358.1.

Wen, G., A. Protat, P. T. May, X. Wang, and W. Moran, 2015: A cluster-based method for hydrometeor classification using polarimetric variables. Part I: Interpretation and analysis. *J. Atmos. Oceanic Technol.*, **32**, 1320–1340, doi:10.1175/JTECH-D-13-00178.1.

Zrnić, D., and A. Ryzhkov, 1999: Polarimetry for weather surveillance radars. *Bull. Amer. Meteor. Soc.*, **80**, 389–406, doi:10.1175/1520-0477(1999)080<0389:PFWSR>2.0.CO;2.

——, V. Bringi, N. Balakrishnan, K. Aydin, V. Chandrasekar, and J. Hubbert, 1993: Polarimetric measurements in a severe hailstorm. *Mon. Wea. Rev.*, **121**, 2223–2238, doi:10.1175/1520-0493(1993)121<2223:PMIASH>2.0.CO;2.

——, A. Ryzhkov, J. Straka, Y. Liu, and J. Vivekanandan, 2001: Testing a procedure for automatic classification of hydrometeor types. *J. Atmos. Oceanic Technol.*, **18**, 892–913, doi:10.1175/1520-0426(2001)018<0892:TAPFAC>2.0.CO;2.